



LAWRENCE  
LIVERMORE  
NATIONAL  
LABORATORY

# Nonlinear simulations of peeling-ballooning modes with anomalous electron viscosity and their role in ELM crashes

X.Q.Xu, B.Dudson, P.B.Snyder, M.V.Umansky,  
H.Wilson

April 1, 2010

Physical Review Letter

## **Disclaimer**

---

This document was prepared as an account of work sponsored by an agency of the United States government. Neither the United States government nor Lawrence Livermore National Security, LLC, nor any of their employees makes any warranty, expressed or implied, or assumes any legal liability or responsibility for the accuracy, completeness, or usefulness of any information, apparatus, product, or process disclosed, or represents that its use would not infringe privately owned rights. Reference herein to any specific commercial product, process, or service by trade name, trademark, manufacturer, or otherwise does not necessarily constitute or imply its endorsement, recommendation, or favoring by the United States government or Lawrence Livermore National Security, LLC. The views and opinions of authors expressed herein do not necessarily state or reflect those of the United States government or Lawrence Livermore National Security, LLC, and shall not be used for advertising or product endorsement purposes.

# Nonlinear simulations of peeling-ballooning modes with anomalous electron viscosity and their role in ELM crashes

X. Q. Xu<sup>1</sup>, B. Dudson<sup>2</sup>, P. B. Snyder<sup>3</sup>, M. V. Umansky<sup>1</sup>, H. Wilson<sup>2</sup>

<sup>1</sup>*Lawrence Livermore National Laboratory,  
Livermore, CA 94550 USA*

<sup>2</sup>*University of York, Heslington, York YO10 5DD, UK*

<sup>3</sup>*General Atomics, San Diego, CA 92186 USA*

A minimum set of equations based on the Peeling-Ballooning (P-B) mode with non-ideal physics effects (diamagnetic drift, ExB drift, resistivity, and anomalous electron viscosity) is found to simulate pedestal collapse when using the new BOUT++ simulation code, developed in part from the original fluid edge code BOUT. Nonlinear simulations of P-B modes demonstrate that the P-B modes trigger magnetic reconnection, which may be related to the partial collapse of the pedestal found in the simulations. With addition of a model of the anomalous electron viscosity under the assumption that the anomalous kinematic electron viscosity is comparable to the anomalous electron thermal diffusivity, it is found from simulations using a realistic high Lundquist number that the pedestal collapse is limited to the edge region and the ELM size is about 5-10% of the pedestal stored energy. This is consistent with many observations of large ELMs.

PACS numbers: 52.55.Fa, 52.25.Fi, 52.35.Ra, 52.65.Tt, 52.65.Kj

The problem of fast reconnection in high-Lundquist number plasmas has attracted a great deal of attention, in large part due to its relevance to impulsive phenomena such as magnetospheric substorms, solar and stellar flares, sawtooth crashes and edge localized modes (ELMs) in tokamaks. Here we report fast-reconnection simulation studies in ELMs in high-confinement mode (H-mode) tokamak discharges [1]. The H-mode pedestal, the region of strongly reduced turbulence and transport just inside the limiting flux surface, is very important for the fusion performance of ITER. The ELMs, however, are quasi-periodic relaxations of the pedestal, resulting in a series of hot plasma eruptions that could potentially damage the ITER divertor plates and first walls.

Through the development of the theory of peeling-ballooning (P-B) modes and their numerical implementation in codes such as ELITE [2,3], a robust prediction of edge MHD stability limits is available for existing and future tokamaks. It has been found that large ELMs are triggered and pedestal height is constrained by ideal P-B stability. P-B modes are ideal MHD modes which are driven by a combination of sharp pressure gradients (ballooning) and bootstrap current in the pedestal. Onset of each ELM (type-I) was consistently found to correlate with crossing of the ideal P-B stability boundary [4], i.e., P-B theory successfully describes the trigger of the ELM. However the nonlinear dynamics, and in particular the physics of the ELM energy loss and pedestal dynamics after the onset of each ELM (type-I) remain uncertain.

Nonlinear ELM simulations become computationally difficult for high Lundquist number due to the fine resolution needed to resolve the narrow current sheet and/or narrowing fingers as a result of explosive ideal MHD instabilities predicted from nonlinear ballooning theory [5,6], leading to collapse of the simulation time-step at the early non-linear stage of P-B mode development[6].

A common practice is to use an enhanced resistivity and/or ion viscosity to achieve nonlinear ELM simulations, which leads to significantly different linear growth rates and instability thresholds. Furthermore, in nonlinear resistive MHD simulations, the pedestal pressure collapses deep into the plasma core, which yields much larger Elm sizes than observed.

In the present Letter, we describe three-fields nonlinear simulations of plasma edge pedestal collapse in the tokamak configuration. The simulations are carried out in the BOUT++ two-fluid framework [7], which allows studies of nonlinear dynamics of ELMs including extensions beyond MHD physics. Based on the P-B model with non-ideal physics effects (diamagnetic drift, ExB drift, resistivity, and anomalous electron viscosity), a minimum set of nonlinear equations for perturbations of the magnetic flux  $A_{\parallel}$ , electric potential  $\phi$ , and pressure  $P$  can be extracted from a complete set of BOUT two-fluids equations [8] with an additional effect of hyper-resistivity [9]. This can be written as

$$\frac{\partial \varpi}{\partial t} + \mathbf{v}_{\mathbf{E}} \cdot \nabla \varpi = B_0 \nabla_{\parallel} J_{\parallel} + 2\vec{b}_0 \times \vec{\kappa}_0 \cdot \nabla P \quad (1)$$

$$\frac{\partial P}{\partial t} + \mathbf{v}_{\mathbf{E}} \cdot \nabla P = 0 \quad (2)$$

$$\frac{\partial A_{\parallel}}{\partial t} = -\nabla_{\parallel} \Phi + \frac{\eta}{\mu_0} \nabla_{\perp}^2 A_{\parallel} - \frac{\eta_H}{\mu_0} \nabla_{\perp}^4 A_{\parallel} \quad (3)$$

$$\varpi = \frac{n_0 M_i}{B_0} \left( \nabla_{\perp}^2 \phi + \frac{1}{n_0 Z_i e} \nabla_{\perp}^2 P \right), \Phi = \phi + \Phi_0,$$

$$J_{\parallel} = J_{\parallel 0} - \frac{1}{\mu_0} \nabla_{\perp}^2 A_{\parallel}, v_E = \frac{1}{B_0} (b_0 \times \nabla_{\perp} \Phi).$$

Here  $\nabla_{\parallel} F = B \partial_{\parallel} (F/B)$  for any  $F$ ,  $\partial_{\parallel} = \partial_{\parallel}^0 + \vec{\mathbf{b}} \cdot \nabla$ ,  $\vec{\mathbf{b}} = \vec{\mathbf{B}}/B = \nabla_{\parallel} A_{\parallel} \times \mathbf{b}_0/B$ ,  $\partial_{\parallel}^0 = \mathbf{b}_0 \cdot \nabla$ ,  $\kappa_0 = \mathbf{b}_0 \cdot \nabla \mathbf{b}_0$ . Although hyper-resistivity  $\eta_H$ , also known as electron vis-

cosity, is generally negligibly small in collisional plasmas, it can be significant in a collisionless plasma. In this model the frozen-in flux constraint of ideal MHD theory is broken by either resistivity or hyper-resistivity.

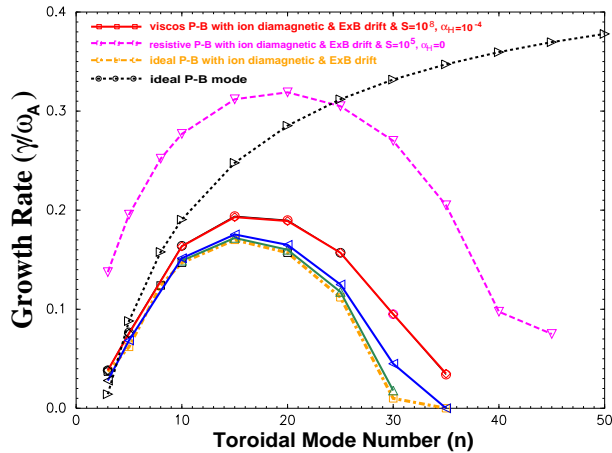


FIG. 1: (Color online) Toroidal mode spectrum of the first equilibrium as calculated by BOUT++ for following cases: ideal MHD (black dotted line), ideal MHD with ExB and diamagnetic drift (yellow square),  $S = 10^5$  and  $S_H = \infty$  (pink inverted triangle),  $S = 10^8$  and  $\alpha_H = 10^{-4}$  (red open circle),  $S = 10^8$  and  $\alpha_H = 10^{-5}$  (blue right triangle),  $S = 10^8$  and  $\alpha_H = 10^{-6}$  (green triangle). The growth rates are normalized to the Alfvén frequency  $\omega_A$ .

To study the physics of nonlinear P-B mode dynamics, we choose circular cross-section toroidal equilibria with an aspect ratio of 2.9 generated by the TOQ equilibrium code. Two model equilibria will be simulated for H-mode plasmas with steep pressure and current gradients at the edge [10]. The first equilibrium is far from the marginal P-B instability threshold with a pedestal toroidal pressure  $\beta_{t0} = 1.941 \times 10^{-2}$  and a normalized pedestal width  $L_{ped}/a = 0.0486$ . The second equilibrium is near the marginal P-B instability threshold with  $\beta_{t0} = 1.45 \times 10^{-2}$  and  $L_{ped}/a = 0.0518$ . Parameters that are held fixed between the two include a minor radius  $a = 1.2\text{m}$ , major radius  $R_0 = 3.4\text{m}$ , toroidal field on axis  $B_0 = 2\text{T}$ , an edge  $q_a \simeq 3$ , the pedestal pressure 2/3 of the axis pressure, and a pedestal half width 7% of the poloidal flux. In this study, the resistivity  $\eta$ , hyper-resistivity  $\eta_H$  and edge density  $n_0 = 1 \times 10^{19}\text{m}^{-3}$  are treated as constants in space-time across simulation domain. In the present simplified model, both equilibrium flow and turbulent zonal flow have been set to be zero:  $\mathbf{V}_0 = \mathbf{V}_{E0} + \mathbf{V}_{\nabla P_i} = 0$  and  $\langle \delta \mathbf{v} \rangle_\zeta = \langle \mathbf{v}_E \rangle_\zeta + \langle \mathbf{v}_{\nabla P_i} \rangle_\zeta = 0$ . Therefore, the equilibrium electric field is  $E_{r0} = (1/n_0 Z_i e) \nabla_r P_{i0}$  with ion pressure  $P_{i0} = P_0/2$ , and the perturbed electric field is  $\langle E_r \rangle_\zeta = (1/n_0 Z_i e) \nabla_r \langle P_i \rangle_\zeta$ . The zonal magnetic field is also set to be zero as it is negligibly small compared to the equilibrium magnetic field  $B_0$ .

The equations (1)-(3) are solved using a field-aligned (flux) coordinate system  $(x, y, z)$  with shifted radial derivatives [7]. Differencing methods used are 4th-order central differencing and 3rd-order WENO advec-

tion scheme. The resulting difference equations are solved with a fully implicit Newton-Krylov solver: Sundials CVODE package. Radial boundary conditions used are:  $\varpi = 0, \nabla_\perp^2 A_\parallel = 0, \partial P / \partial \psi = 0$ , and  $\partial \phi / \partial \psi = 0$  on inner radial boundary;  $\varpi = 0, \nabla_\perp^2 A_\parallel = 0, P = 0$ , and  $\phi = 0$  on outer radial boundary. The domain is periodic in  $y$  (with a twist-shift condition) and periodic in  $z$  (toroidal angle). For efficiency, when performing nonlinear simulations, only 1/5th of the torus is simulated. The number of grid cells in each coordinate are  $n_\psi = 512, n_\theta = 64, n_\zeta = 32$  for linear runs and  $n_\zeta = 64, 128, 256$  for nonlinear runs.

A series of BOUT++ simulations is conducted to investigate the scaling characteristics of the P-B mode as a function of two dimensionless quantities  $S$  and  $S_H$ . One is a  $S$ -scan for a fixed  $S_H = 10^{12}$ , while the other is a  $S_H$ -scan for a fixed  $S = 10^7$  or  $S = 10^8$ . Here the Lundquist number  $S = \mu_0 R_0 v_A / \eta$  is the dimensionless ratio of an Alfvén wave crossing timescale to a resistive diffusion timescale. Here  $v_A$  is the Alfvén velocity. Similarly, the hyper-Lundquist number  $S_H = \mu_0 R_0^3 v_A / \eta_H = S / \alpha_H$  is the dimensionless ratio of an Alfvén wave crossing timescale to a hyper-resistive diffusion timescale, with a dimensionless hyper-Lundquist parameter  $\alpha_H = \eta_H / R_0^2 \eta$ . For a collisional electron viscosity,  $\alpha_H \simeq \mu_e / R_0^2 \nu_{ei}$ . Assuming that the anomalous kinematic electron viscosity  $\mu_e$  is comparable to the anomalous electron thermal diffusivity  $\chi_e$ , for edge plasma parameters  $\mu_e \simeq \chi_e \simeq 1\text{m}^2/\text{s}$  and electron-ion collision frequency  $\nu_{ei} \simeq 10^5/\text{s}$ , we can estimate the amplitude of the hyper-Lundquist parameter to be  $\alpha_H \simeq 10^{-4} - 10^{-6}$ .

Linear simulations of P-B mode evolution find good agreement in growth rate and mode structure with ELITE calculations [2,7]. Fig. 1 shows the growth rate vs toroidal mode number  $n$  of the first equilibrium as calculated by BOUT++ for various cases. The growth rate for ideal MHD P-B mode is plotted as black dotted line. The influence of the  $E \times B$  drift, diamagnetic drift, resistivity, and anomalous electron viscosity on P-B modes is also shown. We find that (1) the diamagnetic drift and ExB drift stabilize the P-B mode (yellow square in Fig. 1) in a manner consistent with theoretical expectations; (2) resistivity destabilizes the P-B mode, leading to resistive P-B mode, (pink inverted triangle for  $S = 10^5$  and  $S_H = \infty$ ); (3) anomalous electron viscosity destabilizes the P-B mode [11], leading to a viscous P-B mode; for a fixed  $S = 10^8$ , red open circle for  $\alpha_H = 10^{-4}$ , blue right triangle for  $\alpha_H = 10^{-5}$ , green triangle for  $\alpha_H = 10^{-6}$ . For all runs of the viscous P-B mode except as otherwise noted,  $S_H = 10^{12}$ . For a fixed  $S = 10^8$ , as  $\alpha_H$  reduces from  $10^{-4}$  to  $10^{-6}$ , both resistive and viscous effects disappear. BOUT++ reduced-MHD modeling of Eqs. (1-3) captures the marginal stability value  $n > 3$ .

Nonlinear simulations of P-B modes at the early nonlinear stage of development reveal that the current sheet narrows with increasing Lundquist numbers. For typical edge parameters, the Lundquist number is around  $S \simeq 10^8 - 10^{10}$ , the growth rate of the P-B mode is around

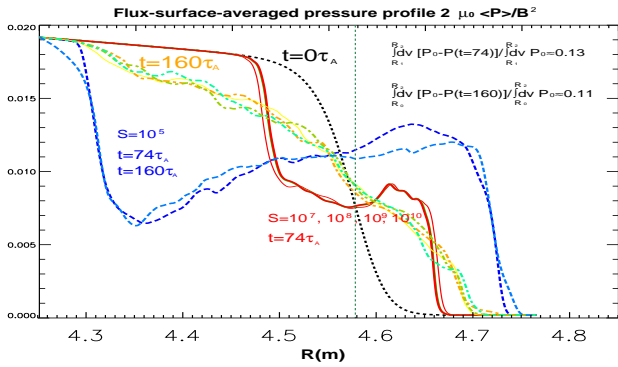


FIG. 2: Radial pressure profiles at several different Lundquist numbers  $S$  and time slices ( $t=0, 74, 160\tau_A$ ) for the first equilibrium: The black dotted line for  $t=0$ ; blue dashed group lines for  $S = 10^5$  at  $t=74\tau_A$  and  $160\tau_A$ ; red solid group lines for  $S \geq 10^7$  at  $t=74\tau_A$ ; yellow dotted-dashed group lines for  $S \geq 10^7$  at  $t=160\tau_A$ . The vertical line indicates the position of peak pressure gradient. Here  $S_H = 10^{12}$ .

$\gamma_{PB} \simeq 0.1\omega_A$ , and the width of the resistive current sheet  $\Delta_J \simeq R\sqrt{\omega_A/\gamma_{PB}/S}$  is around 10-100 microns, which is on the order of a characteristic scale of electron Larmor radius  $\rho_e$ . In the absence of the hyper-resistivity, the simulation time-step collapses as the radial scale-length of the current sheet approaches to the radial grid spacing  $\Delta_x$  for typical resistive MHD simulations  $\Delta_x \gg \Delta_J \simeq \rho_e$ . With the hyper-resistivity, the width of the hyper-resistive current sheet is  $\Delta_H \simeq R(\omega_A/\gamma_{PB}/S_H)^{1/4}$ . The origin of the hyper-resistivity is thought to be small scale electron turbulence in the H-mode pedestal [12]. For the rest of the letter,  $S_H = 10^{12}$ ; hence  $\Delta_H (\simeq 1.78\text{mm}) > \Delta_x (\simeq 1.1\text{mm}) \gg \Delta_J$  with  $\Delta_H/\Delta_J > 17.8$ .

The radial pressure profiles at the outer mid-plane at several different time slices and different Lundquist numbers are shown in Figure 2. It is clearly shown that the pedestal pressure collapses deeply inside the core plasma at low Lundquist number ( $S = 10^5$ ). It is also shown that for high Lundquist number there are two distinct processes in the evolution of pressure profiles: a fast collapse greatly flattening the pressure profile near the peak pressure gradient on the order of tens of Alfvén times after the onset of nonlinear P-B mode,  $t = 74\tau_A$ , and a subsequent slow buildup of pressure gradient. We can characterize the fast collapse as a magnetic reconnection (triggered by P-B modes)  $\rightarrow$  an island formation  $\rightarrow$  bursting process, and a slow buildup as a turbulence transport process. The radial-poloidal pressure profiles clearly show the characteristics of the ballooning mode.

Defining an ELM size as  $\Delta_{ELM} = \Delta W_{PED}/W_{PED} = \langle \int_{R_{in}}^{R_{out}} \oint dRd\theta (P_0 - \langle P \rangle_\zeta) \rangle_t / \int_{R_{in}}^{R_{out}} \oint dRd\theta P_0$ , the ratio of the ELM energy loss ( $\Delta W_{PED}$ ) to the pedestal stored energy  $W_{ped}$  ( $W_{ped} = 3/2 P_{ped} V_{plasma}$ ), the ELM size can be calculated from each nonlinear simulation. Here  $P$  is the pedestal pressure and the symbol  $\langle \rangle_t$  means the average over time ( $\sim 50 - 100\tau_A$ ) and symbol  $\langle \rangle_\zeta$  means the average over bi-normal periodic coordinate. The

TABLE I: Elm sizes vs Lundquist number  $S$  with  $S_H = 10^{12}$ .

S	$10^4$	$10^5$	$10^7$	$10^8$	$10^9$	$10^{10}$
Case 1	47.18%	28.68%	5.04%	4.67%	4.47%	6.07%
Case 1a	50.96%	35.24%	10.67%	10.02%	10.08%	10.20%
Case 2	45.10%	36.66%		0.22%		0.24%
Case 2a	49.31%	51.56%		1.47%		1.42%

lower integral limit is the pedestal inner radial boundary  $R_{in}$ , while the upper limit is the radial position of the peak pressure gradient  $R_{out}$ . Alternatively, the ELM size  $\Delta_{ELM}^a$  can be calculated by radially integrating the pressure profile at the outer mid-plane as done in experiments, which are denoted by case 1a and 2a in Table I and II for equilibrium 1 and 2. The ELM size scaling vs. Lundquist number  $S$  is given in the Table I. For better convergence a small parallel diffusion term is added to Eq. (2) in case 2 and in case 1 for  $S = 10^{10}$ . The large resistivity ( $S \propto \eta^{-1}$ ) yields a large ELM size for both equilibria, which is contradictory to experimental observations in many devices that the relative ELM size scales inversely with pedestal collisionality [13]. However with a fixed hyper-resistivity  $S_H = 10^{12}$ , when  $S > 10^7$ , which is relevant to today's modestly sized tokamaks and ITER, the ELM size is insensitive to the resistivity. The ELM size for the second equilibrium is much smaller than that for the first as expected.

The ELM size scaling vs. dimensionless hyper-Lundquist parameter  $\alpha_H$  is given in the Table II. The ELM size is proportional to the hyper-resistivity. If we assume that the hyper-resistivity scales inversely with pedestal collisionality ( $\eta_H \propto \nu_{ei}^{-\nu}, \nu > 0$ ), then the ELM size scales inversely with pedestal collisionality, which is consistent with experiments in the high Lundquist number regime. In this regard, the hyper-resistivity induced either by dissipative driftwave/electron-temperature-gradient driven modes or electron transport in the presence of stochastic magnetic field in the collisional regime [14] could possibly yield a consistent collisionality.

TABLE II: Elm sizes vs hyper-Lundquist number  $S_H$

$\alpha_H (S_H = S/\alpha_H)$	$10^{-4}$	$6 \times 10^{-5}$	$10^{-5}$	$5 \times 10^{-6}$
Case 1 $S = 10^7$	11.59%	8.45%	5.1%	
Case 1a $S = 10^7$	21.68%	17.97%	10.7%	
Case 2 $S = 10^8$	5.94%		0.22%	0.14%
Case 2a $S = 10^8$	11%		1.47%	1.5%

From Fig. 2 and Table I and II it is reasonable to conclude that the ELM size is determined by the fast collapse due to the magnetic reconnection. Indeed, field line tracing indicates the creation of magnetic islands and stochastic magnetic field during the collapse, as shown

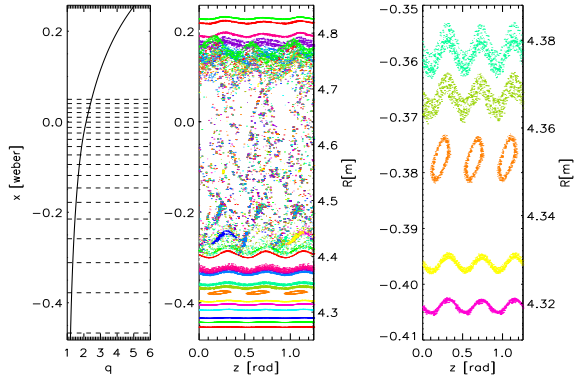


FIG. 3: (a) radial distance  $x$  vs safety factor  $q$ , dashed lines show rational surfaces  $q=m/n$  with  $n=15$ ; (b) line trace for  $S = 10^8$  and  $S_H = 10^{-4}$  during pedestal pressure crash in field-aligned coordinate  $(x,y,z)$ ; (c) a zoom-in view of small region  $x=[-0.41,-0.35]$  in (b) to show the island formation.

in Fig. 3. The size of the fast collapse is proportional to the size of the primary magnetic island at the outer mid-plane near the location of peak pressure gradient. A magnetic island with half-width  $\Delta_{is}$  is defined by  $\Delta_{is}^2 = 4L_s A_{||} / B_0$  with  $L_s = qR/s$ . The estimated island width  $\Delta_{is} \simeq 6.6$  cm at the time of the maximum fast pressure collapse is much wider than the separation distance of the mode rational surfaces  $\Delta_q = (dr/dq)/n$  with mode number  $n=15$ :  $\Delta_{is} \gg \Delta_q$  in the pedestal region; island overlap and magnetic braiding occur, leading to a catastrophic increase of transport, as shown in Fig. 3(b). Further into the core plasma region where perturbed  $A_{||}$  is small, almost good flux surfaces (horizontal curves) and islands can be clearly seen in Fig. 3(c), a zoom-in view of the line trace between  $x=-0.35$  and  $-0.41$ . While for low  $S$  cases, magnetic fluxes are broken everywhere due to large  $A_{||}$  resulting from large magnetic diffusion.

Figure 4 shows the time history of the root-mean-squared  $A_{||rms}$  over the bi-normal coordinate at the outer mid-plane and at the position of peak pressure gradients for both equilibrium 1 and 2. The perturbation grows exponentially from its very small initial value with only one toroidal mode  $n = 15$ . It is clearly shown that the linear growth rate for the first equilibrium is higher than that of the second equilibrium as expected from linear theory and the initial nonlinear saturation amplitude for the first equilibrium is about four times higher than that of second. For the first equilibrium, the time history of  $A_{||rms}$  at the outer mid-plane shows the collapse after the onset of nonlinear saturation at a late time  $t = 105\tau_A$ , while the pressure profile collapses at  $t = 74\tau_A$ . The magnetic fluctuations suddenly start to grow at the onset of the pressure crash. This observation indicates that large ELMs are essentially nonlinear and catastrophic events but evolve from the growth of linear instabilities. The stochastic region is significantly shrunk by the time at  $t = 165\tau_A$  after the ELM event.

In conclusion, the ELM dynamical evolution leads to magnetic reconnection. We find that the magnetic field

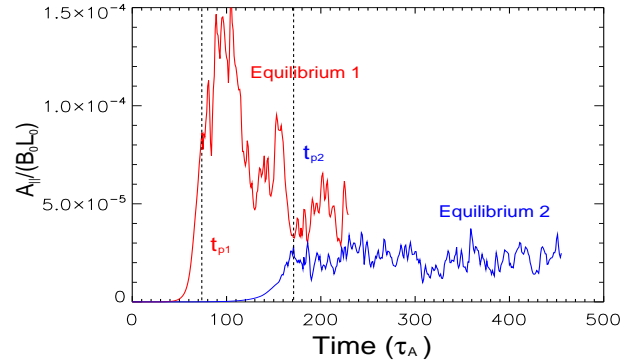


FIG. 4: Time history of the root mean squared  $A_{||}$  at the outer mid-plane and peak pressure gradients for both equilibrium 1 and 2, where  $S = 10^8$ ,  $\alpha_H = 10^{-4}$  for the first equilibrium, and  $\alpha_H = 10^{-5}$  for the second. Pedestal pressure profile collapses at  $t_{p1} = 74\tau_A$  for the first equilibrium and at  $t_{p2} = 171\tau_A$  for the second.

lines must be reconnected before the pedestal pressure profile collapses. With the addition of a model of the anomalous electron viscosity under the assumption that the anomalous kinematic electron viscosity is comparable to the anomalous electron thermal diffusivity to prevent the current sheet from collapsing to the resistive scale-length, it is found from nonlinear simulations that the P-B modes trigger magnetic reconnection. This is believed to drive the partial collapse of the pedestal pressure. For a realistic high Lundquist number, the pedestal collapses are limited to the edge region and the ELM size is about 5-10% of the pedestal stored energy, which is consistent with experimental observations in many devices.

This work was performed for USDOE by LLNL under Contract DE-AC52-07NA27344, grants DE-FG03-95ER54309 at general Atomics, and by the UK Engineering and Physical Sciences Research Council under grant EP/H012605/1 and the Euro. Commun. under the contract of Association between EURATOM and CCFE. The authors wish to acknowledge P.H.Diamond for pointing out the role of the hyper-resistivity in the Ohm's law.

- [1] M. Keilhacker, G. Becker, K. Bernhardt *et al*, Plasma Phys. Control. Fusion 26 49 (1984).
- [2] H. R. Wilson *et al*, Phys. Plasmas 9 (2002) 1277.
- [3] P. B. Snyder *et al*, Phys. Plasmas 9 (2002) 2037.
- [4] P. B. Snyder *et al*, Nucl. Fusion 49 (2009).
- [5] H. R. Wilson *et al*, Phys. Rev. Lett. **92**, 175006 (2004)
- [6] P. B. Snyder *et al*, 2005 Phys. Plasmas 12 056115
- [7] B. D. Dudson, H.R.Wilson, M.V.Umansky, X.Q.Xu, P.B.Snyder, Comput. Phys. Comm.,180,1467 (2009).
- [8] X. Q. Xu *et al*, Comm.in Comput.Phys.4,949(2008).
- [9] P. K. Kaw *et al*, Phys. Rev. Lett. 43, 1398 (1979).
- [10] B. J. Burke *et al*, Phys. Plasmas **17**, 032103 (2010).
- [11] M. Yagi *et al* 1993 Phys. Fluids B 5 3702
- [12] P. H. Diamond, private communication, 2010.
- [13] A. Loarte, G. Saibene, R. Sartori *et al*, 2003 Plasma Phys. Control. Fusion 45 154969.
- [14] A. Rechester *et al*, Phys. Rev. Lett. 40,38(1978).